

Supporting Information

MOF-aminoclay composites for CO₂ capture, separation and enhanced catalytic activity in chemical fixation of CO₂

Anindita Chakraborty, Amritroop Achari, Muthuswamy Eswaramoorthy* and Tapas Kumar Maji*

Chemistry and Physics of Materials Unit, Jawaharlal Nehru Centre for Advanced Scientific Research, Jakkur, Bangalore-560064 (India)

E-mail: eswar@jncasr.ac.in, tmaji@jncasr.ac.in

Synthesis of aminoclay:

Aminoclay was prepared following typical reaction conditions reported by Mann and co-workers [1]. 3-aminopropyltriethoxysilane (1.3 mL, 5.85 mmol) was added dropwise to an ethanolic solution of MgCl_2 (0.84 g, 3.62 mmol) in ethanol (20 g). The white slurry obtained was stirred overnight and the precipitate was isolated by centrifugation and then was washed with ethanol (50 mL) and dried at 40 °C. PXRD pattern (Fig. S1) of the dried compound shows typical reflection corresponding to the d_{001} interlayer spacing of 1.6 nm originating from the bilayer arrangement of propylamine groups.

[1] A. J. Patil, E. Muthusamy and S. Mann, *Angew. Chem. Int. Ed.* 2004, 43, 4928-4933.

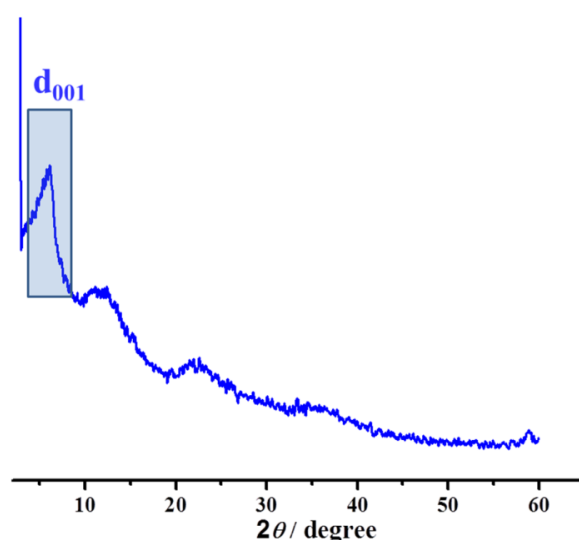


Fig. S1. PXRD pattern of aminoclay. The d_{001} peak is highlighted.

Synthesis of $\{\text{Cu}_3(\text{BTC})_2(\text{H}_2\text{O})_2 \cdot x\text{H}_2\text{O}\}$ (CuBTC) and CuBTC@AC composites:

$\{\text{Cu}_3(\text{BTC})_2(\text{H}_2\text{O})_2 \cdot x\text{H}_2\text{O}\}$ (abbreviated as CuBTC) was prepared by following typical solvothermal reaction conditions. Copper nitrate trihydrate (1 mmol) and 1,3,5 benzenetricarboxylic acid (0.67 mmol) were taken in a mixture of 12 mL DMF, 12 mL ethanol and 8 mL deionized water in a 23 mL teflon-lined stainless steel autoclave and the mixture was stirred for 10 minutes. The autoclave was sealed and was kept in an oven at 80 °C for 24 h. After completion of the reaction, the reactor was cooled at RT for 12 h. The resulting blue product was collected by filtration, washed with DMF and ethanol repeatedly and finally dried. Selected IR data (KBr): $\tilde{\nu} (\text{cm}^{-1}) = 3421$ (br), 2920 (m), 1646 (s), 1590 (m), 1449(s), 1377 (s), 1112 (m), 760 (s), 731 (s), 488 (m). The PXRD pattern of the dried compound shows formation of pure phase of CuBTC (Fig. S2). However, the characteristic

peaks for AC are not observed in the composites due to the fact that AC shows low intensity broad peaks compared to high intensity sharp peaks of CuBTC.

To prepare the **CuBTC@AC-1** composite, first 5 mg of aminoclay (AC) was dispersed in 5 mL of water/ethanol (60: 40) mixture (pH= 7). In aqueous solution, the amine groups of AC are protonated and thus the layers of AC are exfoliated. They can be reverted to their stacked form by the addition of less polar solvents like ethanol. We have taken AC in water/ethanol mixture so that there are sufficient numbers of NH₂ groups (which can bind metal ions) rather than NH₃⁺ ions. Indeed, the dispersed solution of AC in water/ethanol mixture showed smaller positive zeta potential value (12 mV) suggesting the presence of sufficient number of NH₂ groups.

To the dispersed solution of AC in water/ethanol mixture, the precursor solutions of CuBTC are added as described above for the synthesis of CuBTC and similar solvothermal reaction was carried out. The resulting solid was dried after repeatedly washing with ethanol, and is referred to as **CuBTC@AC-1**. Similar procedure was repeated for the synthesis of **CuBTC@AC-2** and **CuBTC@AC-3** where 10 mg and 20 mg of aminoclay were taken, respectively. The weight % of CuBTC in the composites were calculated through Inductively Coupled Plasma-Atomic Spectroscopy (ICP-AES) study based on the relative ratio of Cu(II) in the pristine CuBTC and the composites. Selected IR data for **CuBTC@AC-2**: (KBr): $\tilde{\nu}$ (cm⁻¹) = 3389 (br), 2499 (m), 1647 (s), 1576 (br, s), 1448 (s), 1370 (s), 1114 (s), 1017 (m), 766 (s), 734 (s), 637 (s), 475 (s). The well-correspondence of the PXRD patterns of CuBTC and the composites suggests existence of pure crystalline phase of CuBTC in the composites (Fig. S2).

To check the water dispersibility, same amount (5 mg in 1 mL of water) of both CuBTC and **CuBTC@AC-2** samples were dispersed in water. The dispersion remains stable even after 6 hours for the **CuBTC@AC-2** sample, while the bulk CuBTC precipitates within 15 minutes (Fig. S6).

Control experiments to study the growth and stabilization of CuBTC NPs on the aminoclay:

10 mg of aminoclay (AC) was dispersed in 5 mL of water/ethanol mixture (pH= 7). Copper nitrate trihydrate (1 mmol) was added to the above solution and the mixture was stirred for 10 minutes at room temperature. The green solid product (obtained after precipitation by adding ethanol to the reaction mixture) was washed several times with ethanol and dried. Elemental mapping and EDX analysis of the solid (referred as Cu@AC) show the presence of Cu

distributed uniformly throughout the clay (Fig. S8). This suggests that the Cu(II) ions are strongly bound to the free amine groups of AC. Then Cu@AC solid and BTC linker (0.67 mmol) were mixed in a 23 mL teflon-lined stainless steel autoclave containing 12 mL DMF, 12 mL ethanol and 8 mL deionized water and the mixture was stirred for 10 minutes. The autoclave was sealed and was kept in an oven at 80 °C for 24 h. After completion of the reaction, the reactor was cooled at RT for 12 h. The resulting blue product was collected by filtration, was washed with DMF and ethanol repeatedly and finally was dried. The PXRD pattern of the resulting composite reveals formation of the pure phase of CuBTC (Fig. S9).

Physical measurements:

¹H NMR data were measured on a Bruker AV-400 spectrometer with chemical shifts reported as ppm (TMS as internal standard). Powder X-ray diffraction (PXRD) patterns were recorded on a Bruker D8 Discover instrument using Cu-K α radiation. Inductively Coupled Plasma-Atomic Emission Spectroscopy (ICP-AES) measurements were recorded on Perkin Elmer Optima 7000dv ICP-AES instrument. Energy dispersive analysis of X-rays (EDX) was carried out using field emission scanning electron microscope. The scanning electron microscopy images were obtained using a Nova Nanosem 600 FEI field emission scanning electron microscope (FESEM). The samples were prepared by dispersing the sample in MeOH and then dropping 5 μ L of the solution onto a small piece of silicon wafer and drying into air. Transmission electron microscopy (TEM) images were taken with a JEOL JEM-3010 transmission electron microscope operating at 200 kV. The samples were prepared in the same way as described above, but the drop cast was made onto a carbon-coated TEM grid.

Adsorption measurements:

Adsorption isotherms of N₂ (at 77K, 298 K), CO₂ (at 273 K and 298 K) and CH₄ (at 298 K) were recorded with the desolvated samples using QUANTACHROME QUADRASORB-SI analyser and AUTOSORB IQ2 instrument. To prepare the desolvated samples of CuBTC and the composites, approximately 70 mg of sample was degassed at 160 °C under 10⁻¹ pa vacuum for about 8 hours prior to the measurements. Dead volume of the sample cell was measured with helium gas of 99.999% purity. The MeOH adsorption isotherms were measured at 298 K in the gaseous state by using BELSORP-aqua-3 analyzer. All operations were computer controlled and automatic. The kinetic data were fitted into the linear driving force mass transfer (LDF) model which can be described by the equation: $M_t/M_e = 1 - \exp(-kt)$, where M_t and M_e are the mass uptake at time t and at equilibrium respectively,

and k is the kinetic rate constant. To ensure equilibrium, the adsorption kinetics measurements were performed with sufficient equilibrium time (1500 seconds). The adsorption rate graph and the kinetic data were analysed using BELDyna software.

Breakthrough column experiments:

Breakthrough experiments were performed using a column (packed with about 150 mg of desolvated samples) of 1 cm long length and 0.3 cm diameter. The sample was first activated (at 160 °C under 10^{-1} pa vacuum for about 8 hours) prior to loading in column. For both CuBTC and **CuBTC@AC-2**, the same amount of samples (150 mg, column length is 1 cm) was used. After loading the sample was again activated with the He flow for 30 minutes. CO₂/N₂ (V/V: 15/85) and CO₂/CH₄ (V/V: 50:50) streams were passed from the corresponding gas cylinders containing the gas mixtures through the column with He. The flow was continuous and the flow rate was regulated by mass flow controller (MFC). The rate of the flow (He: binary gas mixture = 90: 10) was fixed at 1 ml/min. The gas stream at the outlet of the column was analyzed on-line with a GC.

Catalysis study:

The catalyst was activated (at 160 °C under 10^{-1} pa vacuum for about 8 hours) prior to the catalysis reaction. The catalytic reaction was conducted in a Schlenk tube using propylene oxide (25 mmol) with CO₂ purged at 1 atm under solvent free environment at room temperature catalyzed by the activated catalyst (0.125 mol% calculated based on copper paddlewheel units; 0.03125 mmol for CuBTC) and co-catalyst of tetra-*n*-tertbutylammonium bromide (TBAB, 0.58g) for 48 hours. Catalytic reaction of 1,2-epoxybutane with CO₂ was performed using similar synthetic condition. After the reaction, the product was collected by adding CHCl₃ and the solid catalyst was removed by centrifuge. The yield was calculated based on ¹H NMR analysis (Fig. 18-22). To perform the recyclability tests, the recovered catalyst was washed with fresh CHCl₃ thoroughly and was dried in air first and then activated at 160 °C under 10^{-1} pa vacuum for 8 hours to perform further reactions under identical conditions.

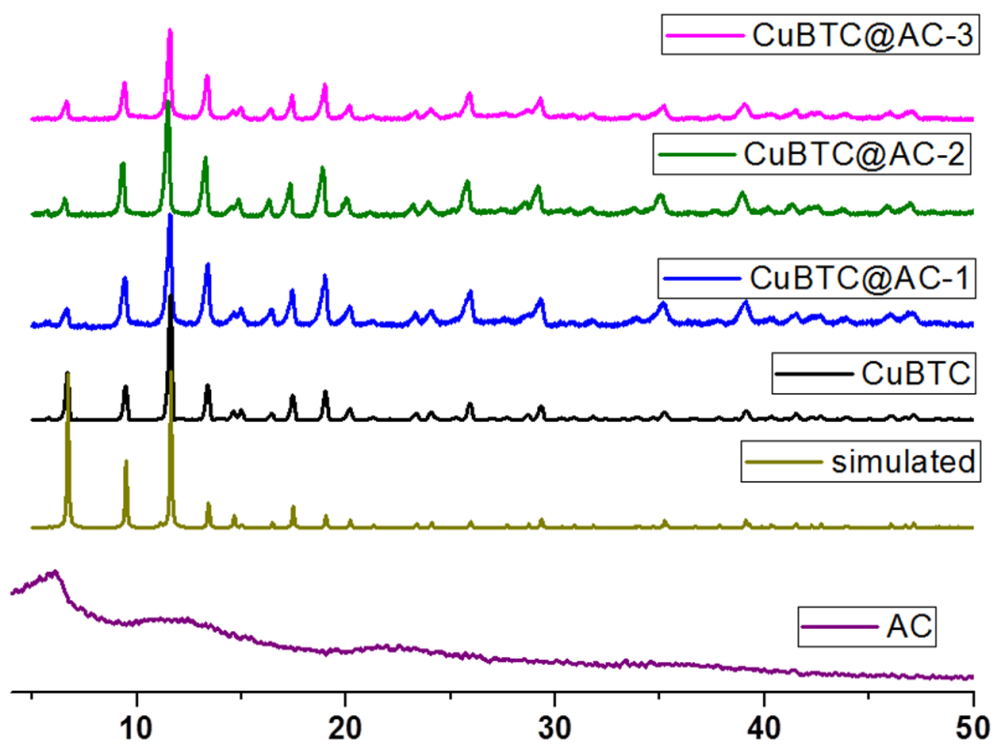


Fig. S2. PXRD patterns of AC, simulated CuBTC, as-synthesized bulk CuBTC and different composites.

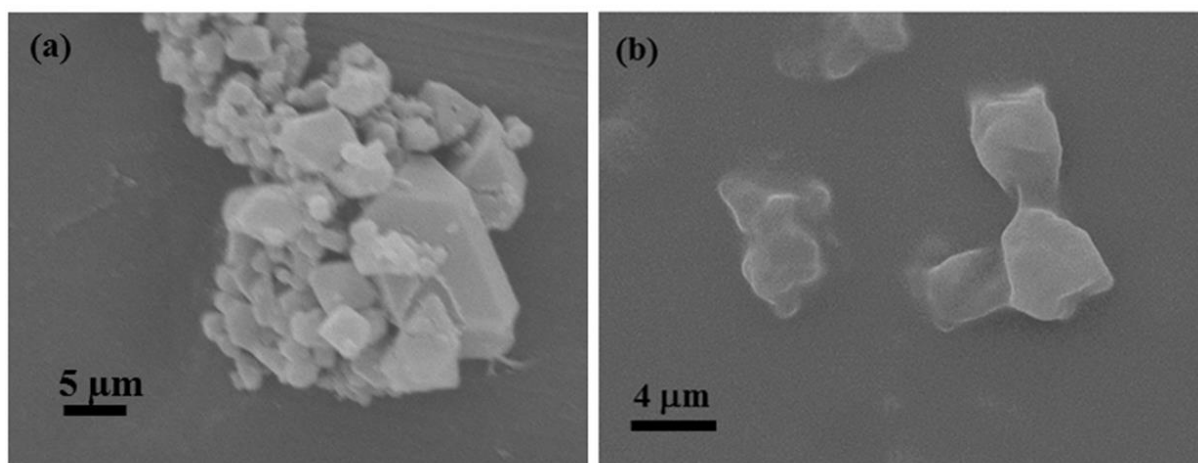


Fig. S3. FESEM images of (a) as-synthesized bulk CuBTC and (b) AC.

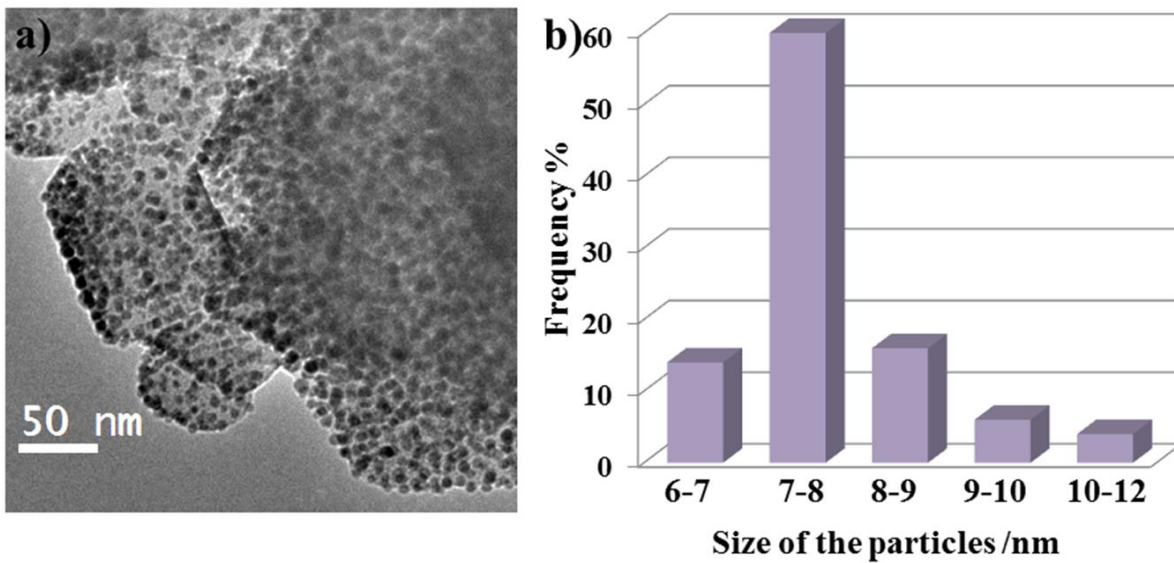


Fig. S4. (a) TEM image of **CuBTC@AC-1** and (b) the size distribution histogram plot showing narrow distribution.

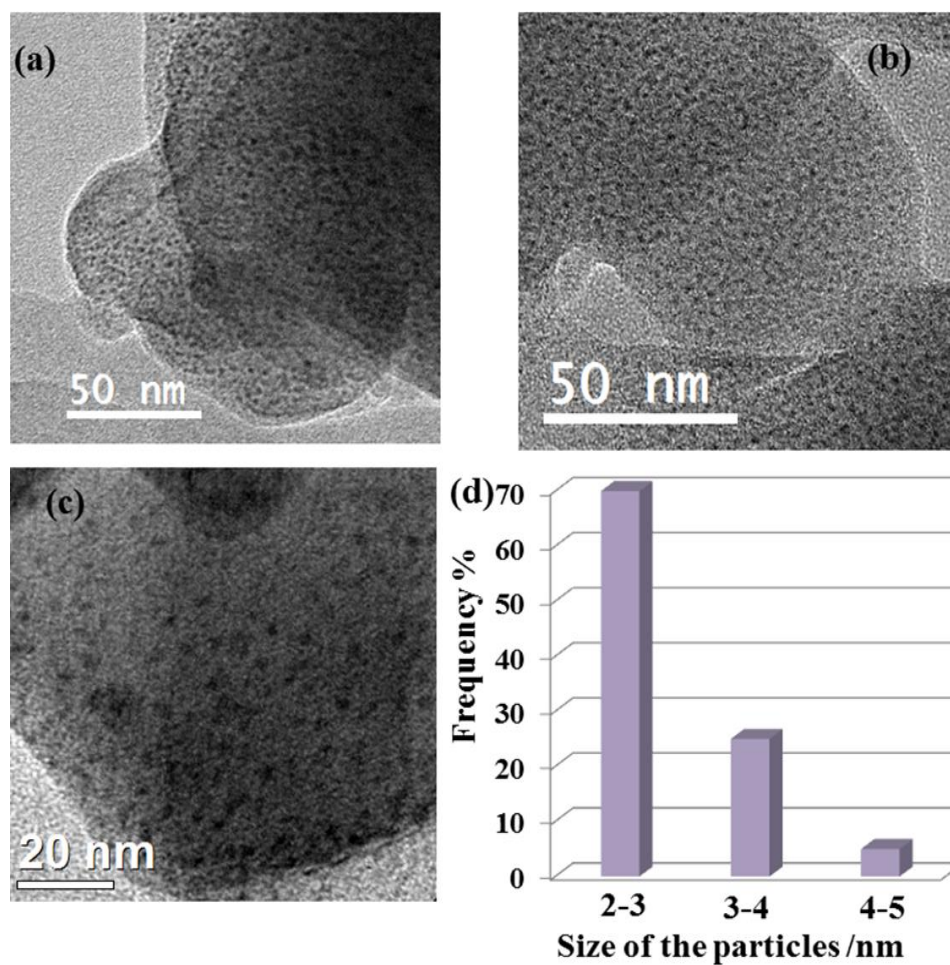


Fig. S5. (a), (b) TEM and (c) HRTEM images of **CuBTC@AC-2** showing monodisperse CuBTC NPs distributed on the layered AC matrix. (d) The size distribution histogram plot showing narrow distribution.

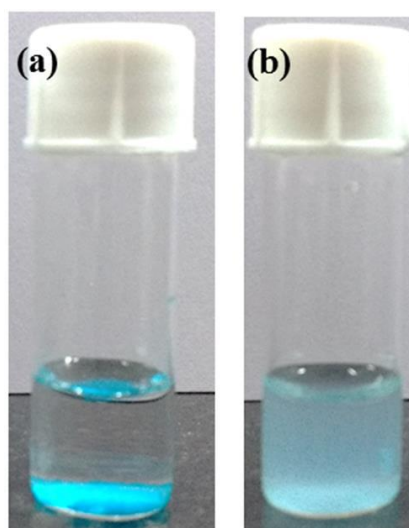


Fig. S6. Images of the solutions of (a) CuBTC after 15 minutes of preparation of dispersion and (b) **CuBTC@AC-2** after 6 hours of preparation of dispersion.

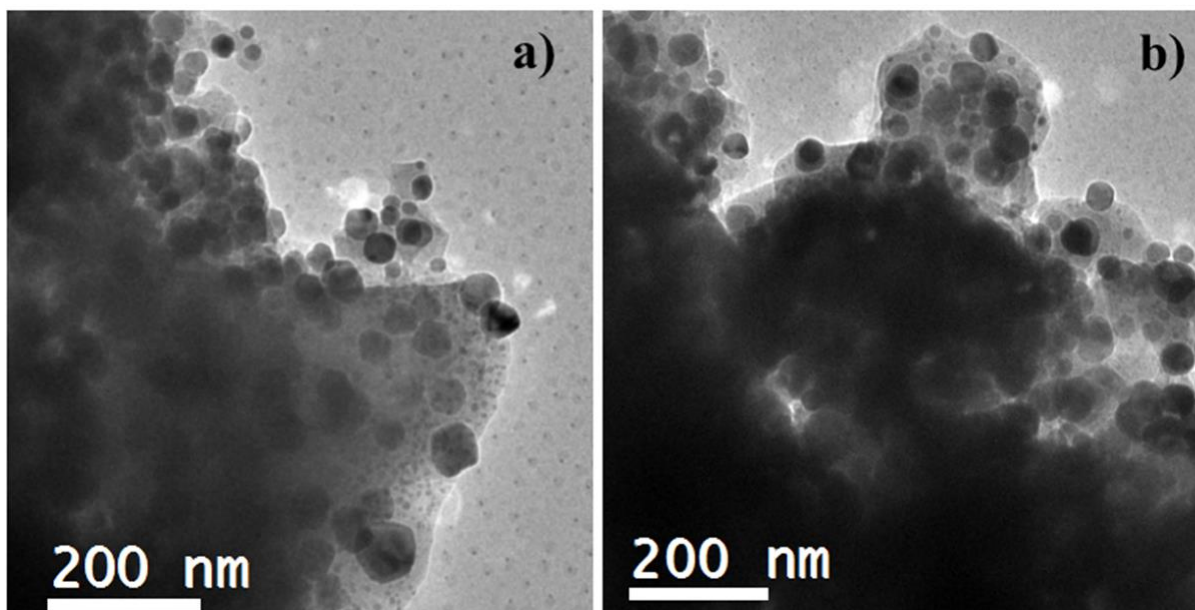


Fig. S7. (a), (b) TEM images of **CuBTC@AC-3**

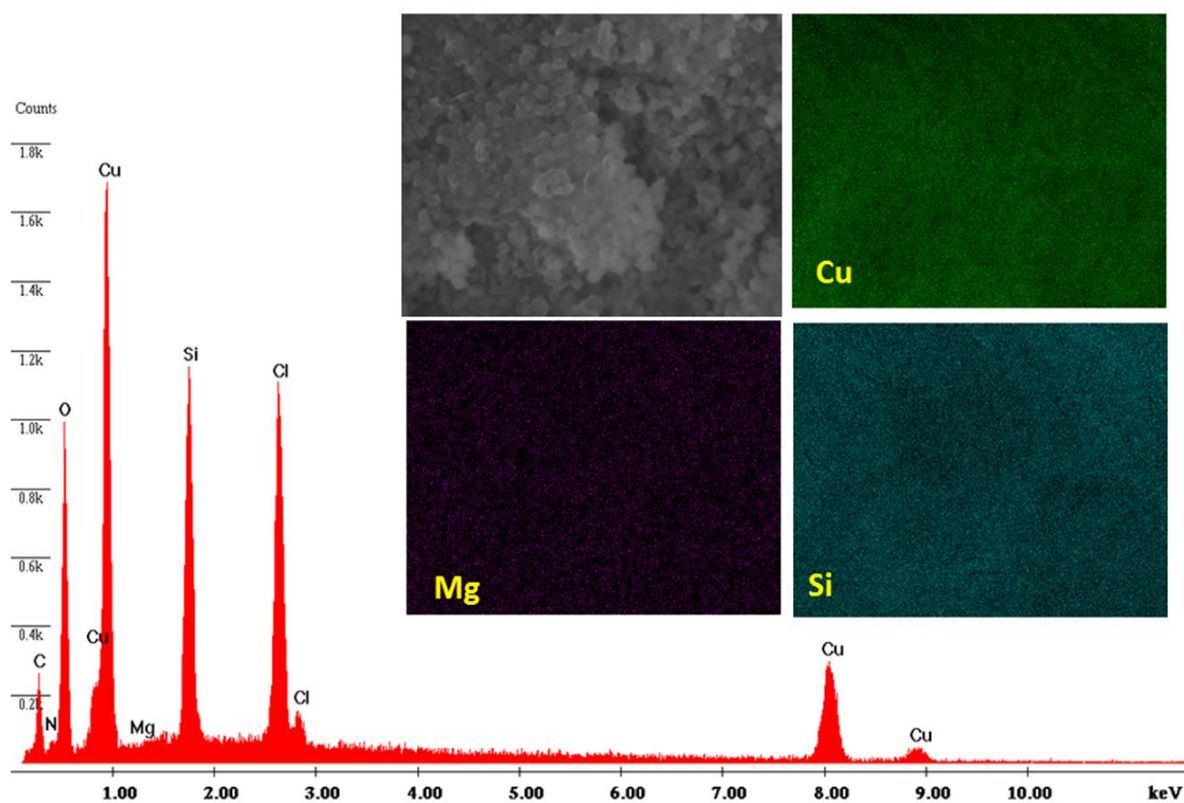


Fig. S8. EDX spectrum of the **Cu@AC** solid showing the presence of **Cu**. Inset shows elemental mapping showing the homogeneous distribution of the elements (**Si**, **Mg** and **Cu**) throughout the sample.

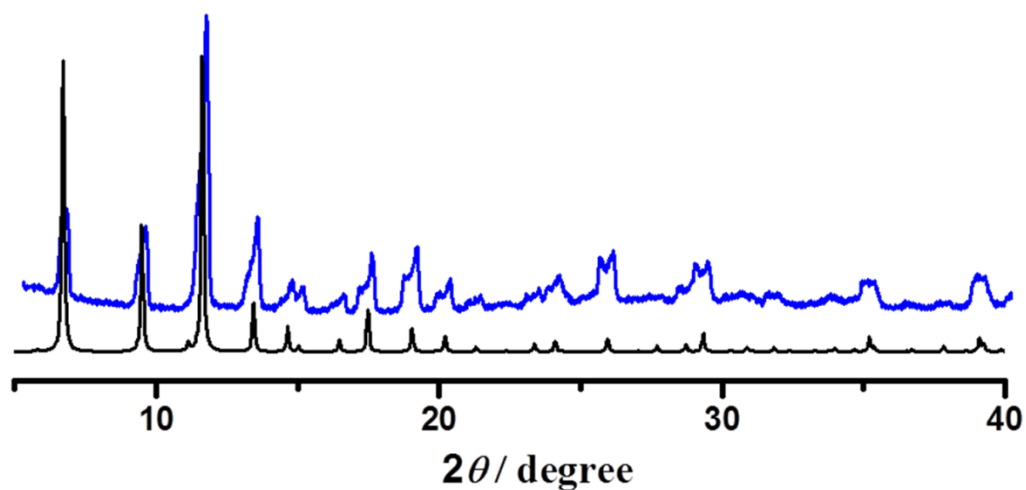


Fig. S9. PXRD patterns of simulated (black) and the solid (blue) obtained from the solvothermal reaction of Cu@AC and BTC linker.

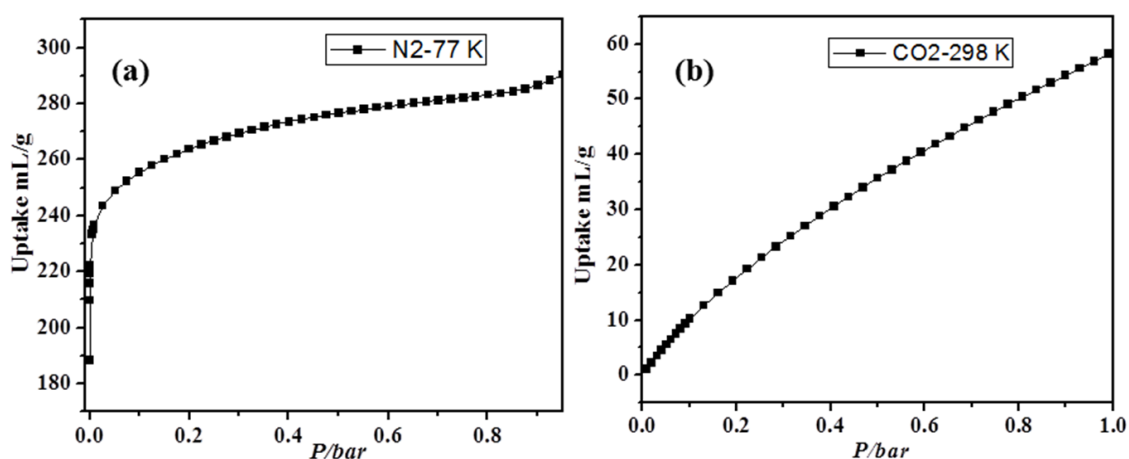


Fig. S10. Adsorption isotherms of the physical mixture of CuBTC and AC (90.4: 9.6 wt%); similar to **CuBTC@AC-2**: (a) N₂ adsorption isotherm at 77 K; (b) CO₂ adsorption isotherm at 298 K. The lesser adsorption uptake compared to CuBTC is attributed to the presence of non-porous AC component. The lesser uptake of the physical mixture suggests that the effect of composite is not realized.

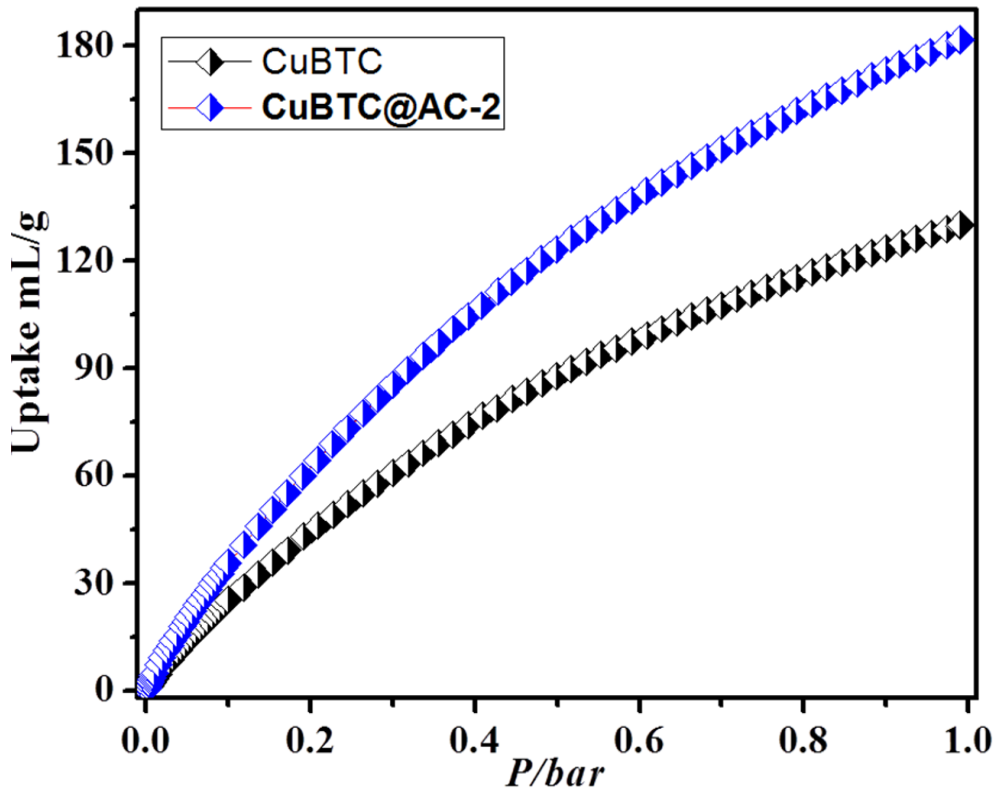


Fig. S11. CO₂ adsorption isotherms of activated CuBTC and CuBTC@AC-2 at 273 K. Open and closed symbol denotes adsorption and desorption respectively.

Determination of isosteric heat of adsorption: Virial fitting of pure component isotherms:

Adsorption isotherms are fitted to the virial-type expression (eq 1).^[1] An accurate fit was obtained for each case which results a precise prediction over the quantity of gas adsorbed at saturation.

$$\ln P = \ln N + 1/T \sum_{i=0}^m a_i N^i + \sum_{i=0}^n b_i N^i \quad \dots\dots\dots(1)$$

$$Q_{st} = -R \sum_{i=0}^m a_i N^i \quad \dots\dots\dots(2)$$

Here, P is the pressure expressed in torr, N is the amount adsorbed in mmol g⁻¹, T is the temperature in K, a_i and b_i are virial coefficients, and m , n represent the number of coefficients required to adequately describe the isotherms. The values of m and n were gradually increased until the contribution of extra added a and b coefficients were negligible towards the overall final fit. The values of the virial coefficient a_i were taken to

calculate the isosteric heat of adsorption using eq 2 (the value of the best fit parameter are presented in the inset of the following Fig.s showing the pure component CO₂ isotherms at 273 K and 298 K fitted into virial-type expression). At zero loading, the isosteric heat of adsorption (Q_{st}) for CuBTC and **CuBTC@AC-2** are 24 and 38 kJ mol⁻¹ respectively.

[1] (a) M. Dincă, A. Dailly, Y. Liu, C. M. Brown, D. A. Neumann and J. R. Long, *J. Am. Chem. Soc.*, 2006, **128**, 16876-16883; (b) J. L. C. Rowsell, O. M. Yaghi, *J. Am. Chem. Soc.*, 2006, **128**, 1304-1315; (c) N. Sikdar, S. Bonakala, R. Haldar, S. Balasubramanian and T. K. Maji, *Chem. Eur. J.*, 2016, **22**, 6059 – 6070.

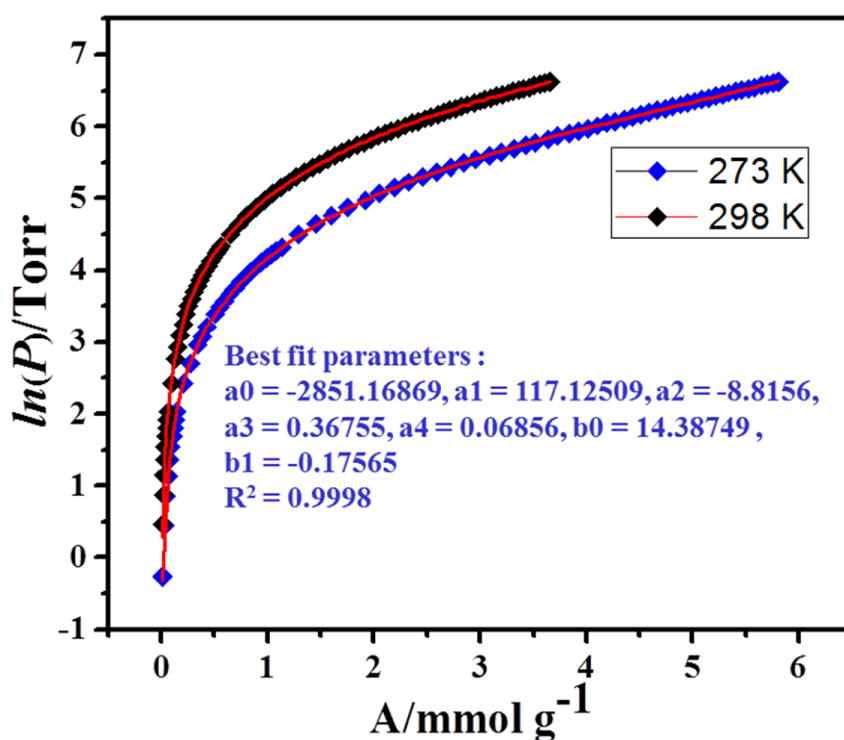


Fig. S12. Pure component CO₂ isotherms of CuBTC at 273 K and 298 K fitted into virial-type expression. The solid red line indicates the best fitting using virial equation.

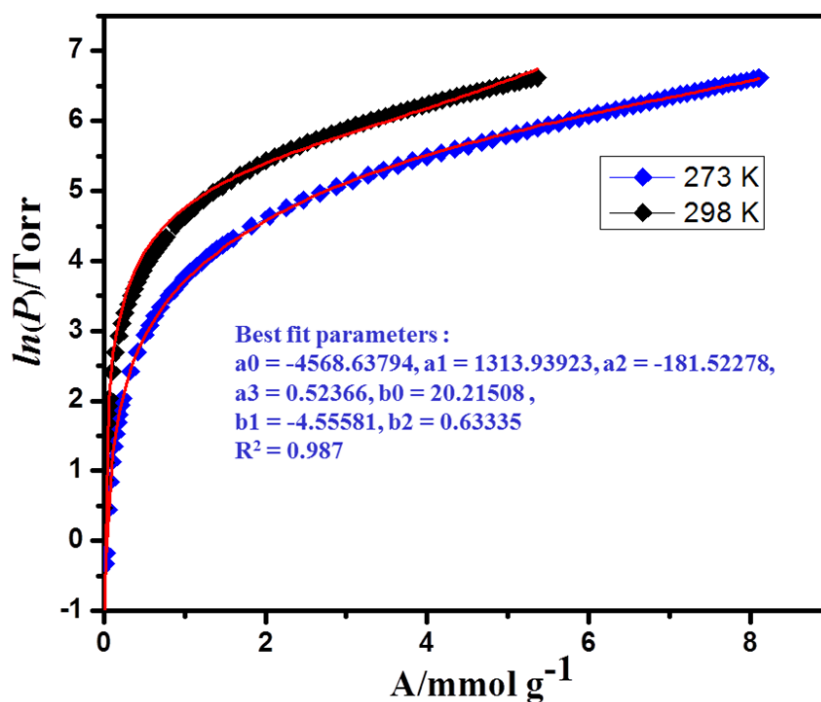


Fig. S13. Pure component CO₂ isotherms of **CuBTC@AC-2** at 273 K and 298 K fitted into virial-type expression. The solid red line indicates the best fitting using virial equation.

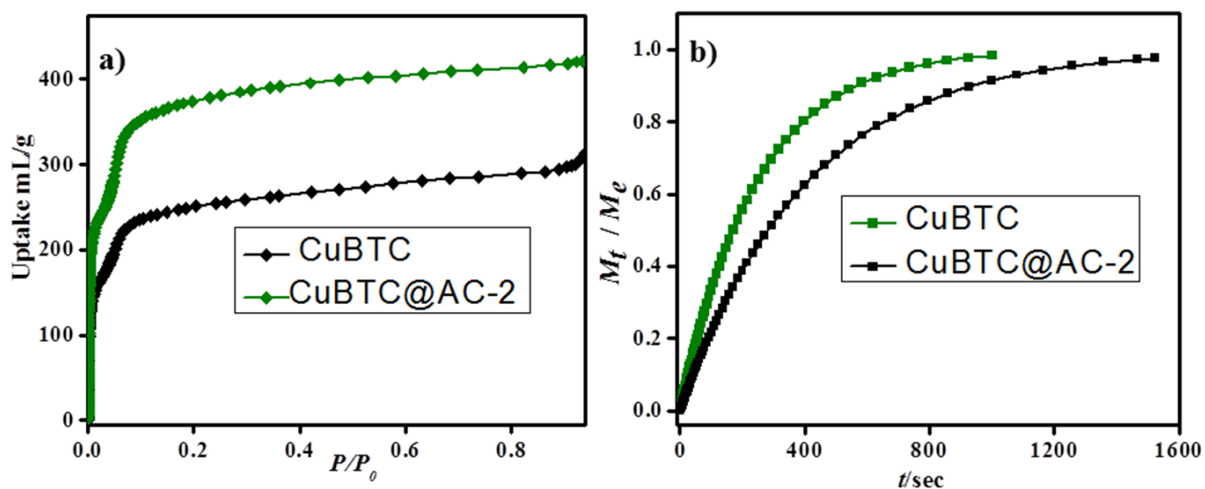


Fig. S14. (a) MeOH vapor adsorption isotherms at 298 K. (b) Kinetics of adsorption of MeOH at 298 K (fitted into LDF model) showing higher mass diffusion in **CuBTC@AC-2** compared to bulk CuBTC.

Table S1: Selected MOFs and their CO₂ adsorption uptake at 298 K, 1 bar

Compounds	CO ₂ uptake at RT, 1 bar (wt%)	Feature of the compound	Reference
Mg ₂ (dobdc), MOF-74-Mg	36.5	Open metal sites (OMS)	1
[Cu ₃ (L1)(H ₂ O) ₃], NU-100 ^a	12	OMS	2
[Zn ₂ L ₃ (H ₂ O)]Cl ^a	17.8	OMS	3
NOTT-140	18.3	OMS	4
Cr ^{III} ₃ O(H ₂ O) ₂ F[C ₁₀ H ₄ (CO ₂) ₄] _{1.5} , MIL-102	13.6	OMS	5
Mg ₂ (dobpdc) ^a	28.25	OMS	6
Cu ₃ (BHB), UTSA-20 ^a	22.4	OMS	7
[Zn ₈ (Ad) ₄ (BPDC) ₆ O], Bio-MOF-1 ^a	14.3	Lewis basic site (LBS)	8
TEA@Bio-MOF-1 ^a	18.3	LBS	9
UiO-66-NH ₂	11.79	LBS	10
[CuL4] ^a	21.8	LBS	11
[Zn(CN ₄ -NH ₂) ₂], ZTF-1	16.68	LBS	12
Cu(4,4'-bipyridine) ₂ (SiF ₆)	23.1	-F functional groups	13
Zn(nbIm)(nIm), ZIF-78 ^a	11.39	-NO ₂ functional groups	14
H ₃ [(Cu ₄ Cl) ₃ (BTTri) ₈], CuBTTri ^a	16.4	OMS and LBS	15
Cu-TDPAT ^a	25.9	OMS and LBS	16
[Cu ₂ (bdcppi)(dmf) ₂], SNU-50 ^a	15.84	OMS and LBS	17
[Cu(Me-4py-trz-ia)] ^a	26.84	OMS and LBS	18
CuBTC	16.1 (82 ml/g); 13.52	OMS	This work; reference 19
CuBTC@AC-2	23.6 (120 ml/g)	OMS, ultra-small MOF NPs, aminopropyl groups at MOF NP-AC interface	This work

^aL1 = 1,3,5-tris[(1,3-carboxylic acid-5-(4-(ethynyl)phenyl))ethynyl]-benzene; L3 = 1,4,7-tris(4-carboxybenzyl)-1,4,7-triazacyclononane); dobdc = 2,5-dioxido-1,4-benzenedicarboxylate; dobpdc = 4,4'-dioxido-3,3'-biphenyldicarboxylate; BHB = 3,3',3'',5,5',5''-benzene-1,3,5-triylhexabenzic acid; ad = adeninate; BPDC = biphenyldicarboxylate; TEA = tetraethylammonium; L4 = 5-(1H-tetrazol-1-yl)isophthalic acid; nbIm = 5-

nitrobenzimidazole; nIm = 2-nitroimidazole; BTTri = 1,3,5-tris(1H-1,2,3,-triazol-5-yl)benzene; TDPAT = 2,4,6-tris(3,5-dicarboxylphenyl-amino)-1,3,5-triazine; bdcppi = N,N0-bis(3,5-dicarboxyphenyl)pyromellitic diimide; Me-4pyz-trz-ia = 5-(3-methyl-5-(pyridine-4-yl)-(4H-1,2,4-triazol-4-yl)isophthalate).

1. S. R. Caskey, A. G. Wong-Foy and A. J. Matzger, *J. Am. Chem. Soc.*, 2008, **130**, 10870–10871.
2. K. Farha, A. O'zgu'r Yazaydin, I. Eryazici, C. D. Malliakas, B. G. Hauser, M. G. Kanatzidis, S. T. Nguyen, R. Q. Snurr and J. T. Hupp, *Nat. Chem.*, 2010, **2**, 944–948.
3. G. Ortiz, S. Brande's, Y. Rousselin and R. Guilard, *Chem.Eur. J.*, 2011, **17**, 6689–6695.
4. C. Tan, S. Yang, N. R. Champness, X. Lin, A. J. Blake, W. Lewis and M. Schroder, *Chem. Commun.*, 2011, 47, 4487–4489.
5. S. Surble', F. Millange, C. Serre, T. Du'ren, M. Latroche, S. Bourrelly, P. L. Llewellyn, G. Fe'rey, *J. Am. Chem. Soc.*, 2006, **128**, 14889–14896.
6. T. M. McDonald, W. R. Lee, J. A. Mason, B. M. Wiers, C. S. Hong and J. R. Long, *J. Am. Chem. Soc.*, 2012, **134**, 7056–7065.
7. Z. Guo, H. Wu, G. Srinivas, Y. Zhou, S. Xiang, Z. Chen, Y. Yang, W. Zhou, M. O'Keeffe and B. Chen, *Angew. Chem. Int. Ed.*, 2011, **50**, 3178–3181.
8. J. An, S. J. Geib and N. L. Rosi, *J. Am. Chem. Soc.*, 2009, **131**, 8376–8377.
9. J. An and N. L. Rosi, *J. Am. Chem. Soc.*, 2010, **132**, 5578–5579.
10. Q. Yang, A. D. Wiersum, P. L. Llewellyn, V. Guillerm, C. Serre and G. Maurin, *Chem. Commun.*, 2011, **47**, 9603–9605.
11. S.-M. Zhang, Z. Chang, T.-L. Hu and X.-H. Bu, *Inorg. Chem.*, 2010, **49**, 11581–11586.
12. T. Panda, P. Pachfule, Y. Chen, J. Jiang and R. Banerjee, *Chem. Commun.*, 2011, **47**, 2011–2013.
13. S. D. Burd, S. Ma, J. A. Perman, B. J. Sikora, R. Q. Snurr, P. K. Thallapally, J. Tian, L. Wojtas and M. J. Zaworotko, *J. Am. Chem. Soc.*, 2012, **134**, 3663–3666.
14. R. Banerjee, H. Furukawa, D. Britt, C. Knobler, M. O'Keeffe and O. M. Yaghi, *J. Am. Chem. Soc.*, 2009, **131**, 3875–3877.
15. A. Demessence, D. M. D'Alessandro, M. L. Foo and J. R. Long, *J. Am. Chem. Soc.*, 2009, **131**, 8784–8786.
16. B. Li, Z. Zhang, Y. Li, K. Yao, Y. Zhu, Z. Deng, F. Yang, X. Zhou, G. Li, H. Wu, N. Nijem, Y. J. Chabal, Z. Lai, Y. Han, Z. Shi, S. Feng and J. Li, *Angew. Chem., Int. Ed.*, 2012, **51**, 1412–1415.
17. T. K. Prasad, D. H. Hong and M. P. Suh, *Chem. Eur. J.*, 2010, **16**, 14043–14050.
18. D. La'ssig, J. Lincke, J. Moellmer, C. Reichenbach, A. Moeller, R. Gla'sser, G. Kalies, K. A. Cychoz, M. Thommes, R. Staudt and H. Krautscheid, *Angew. Chem. Int. Ed.*, 2011, **50**, 10344–10348.
19. C. Montoro, E. Garcia, S. Calero, M. A. Perez-Fernandez, A. L. Lopez, E. Barea and J. A. R. Navarro, *J. Mater. Chem.*, 2012, **22**, 10155–10158.

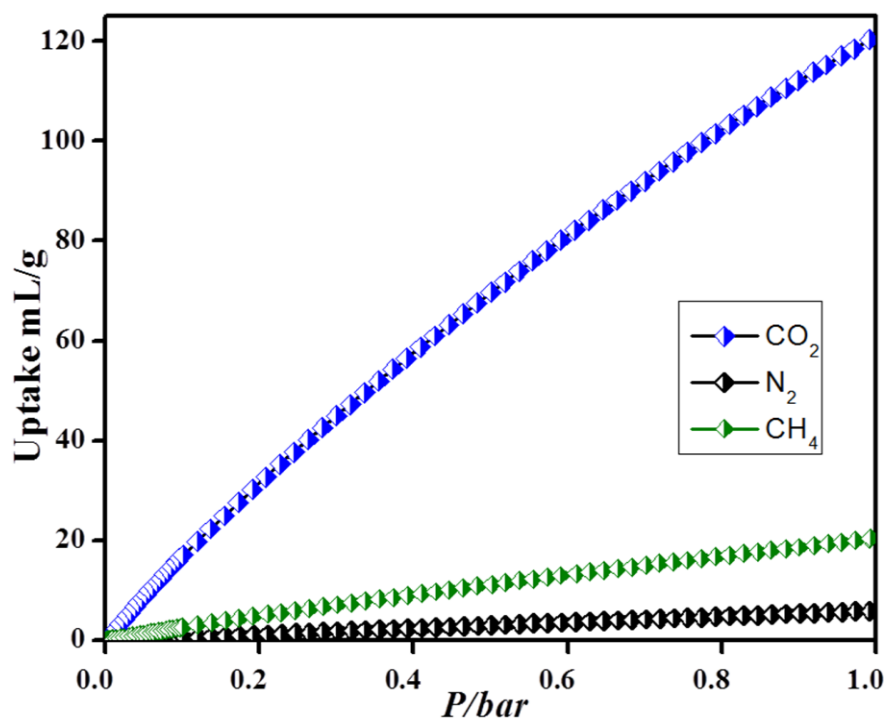


Fig. S15. CO₂, N₂ and CH₄ adsorption isotherms at 298 K of activated CuBTC@AC-2.

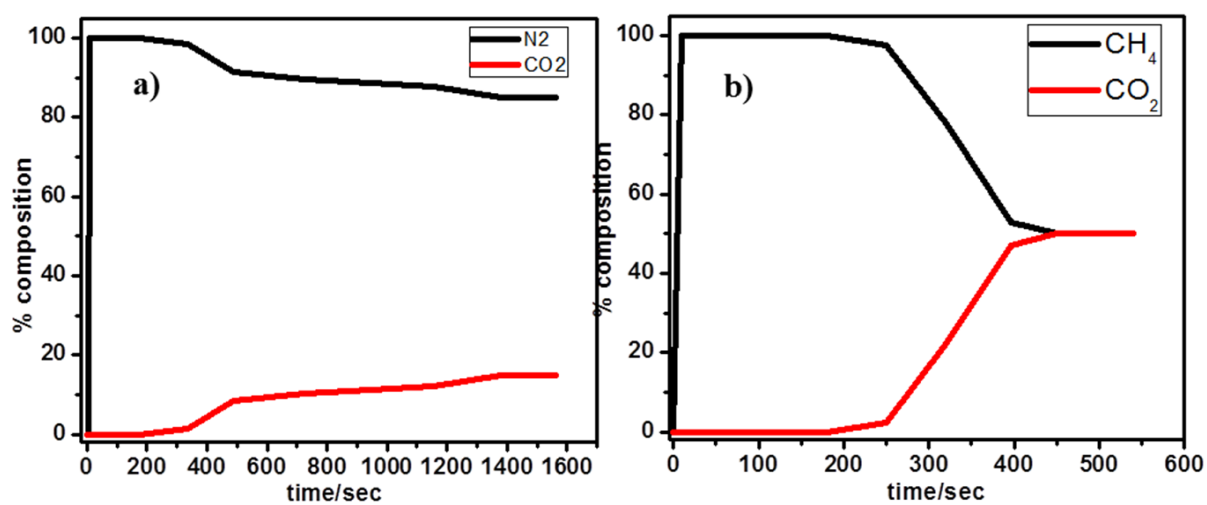


Fig. S16. Breakthrough curves of bulk CuBTC for binary mixture of (a) CO₂ (red)/N₂ (black) (V:V: 15:85) and (b) CO₂ (red)/CH₄ (black) (V:V: 50:50)

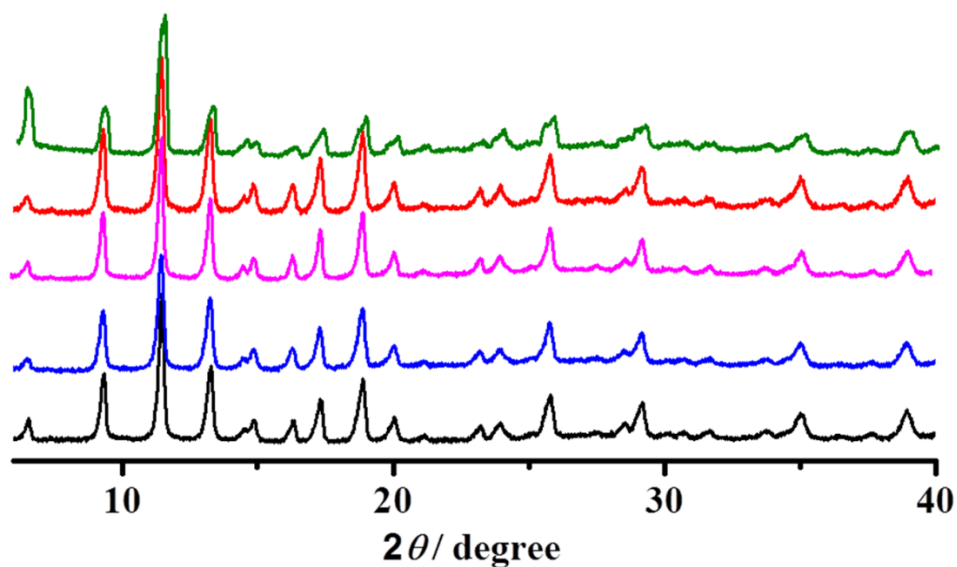


Fig. S17. PXRD patterns of **CuBTC@AC-2** (black) and the recovered catalyst after 1st (blue), 2nd (pink), 3rd (red) and 4th cycle (green) of the catalytic reaction.

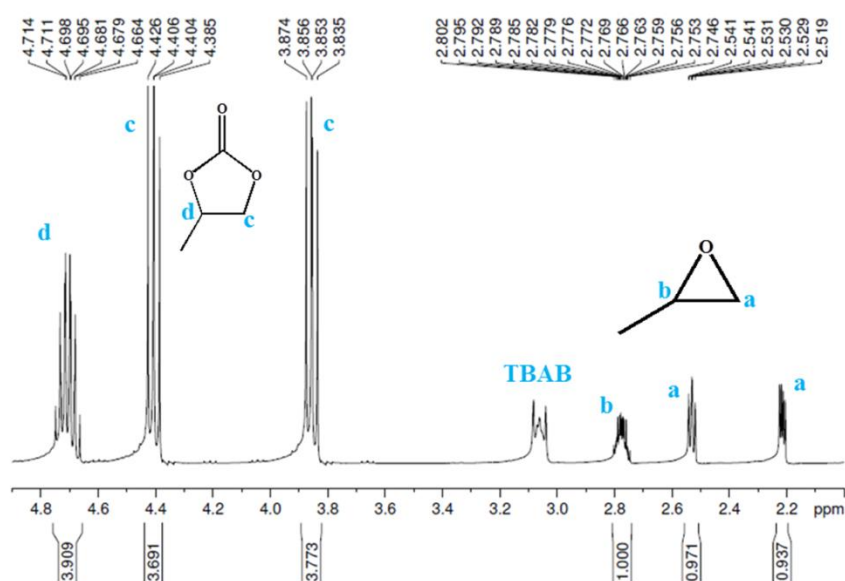


Fig. S18. ¹H-NMR spectra (in CDCl₃) of the reaction mixture using **CuBTC@AC-2** as a catalyst for the cycloaddition reaction of propylene oxide. The peaks corresponding to propylene oxide, propylene carbonate and the co-catalyst tetrabutylammonium bromide (TBAB) have been shown.

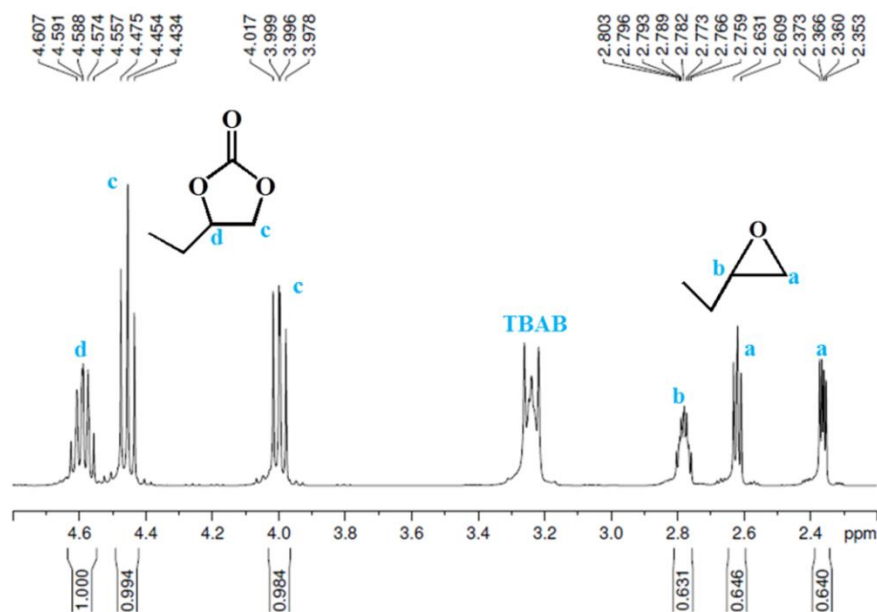


Fig. S19. ¹H-NMR spectra (in CDCl₃) of the reaction mixture using **CuBTC@AC-2** as a catalyst for the cycloaddition reaction of 1,2-epoxybutane. The peaks corresponding to 1,2-epoxybutane, 1,2-butylene carbonate and the co-catalyst tetrabutylammonium bromide (TBAB) have been shown.

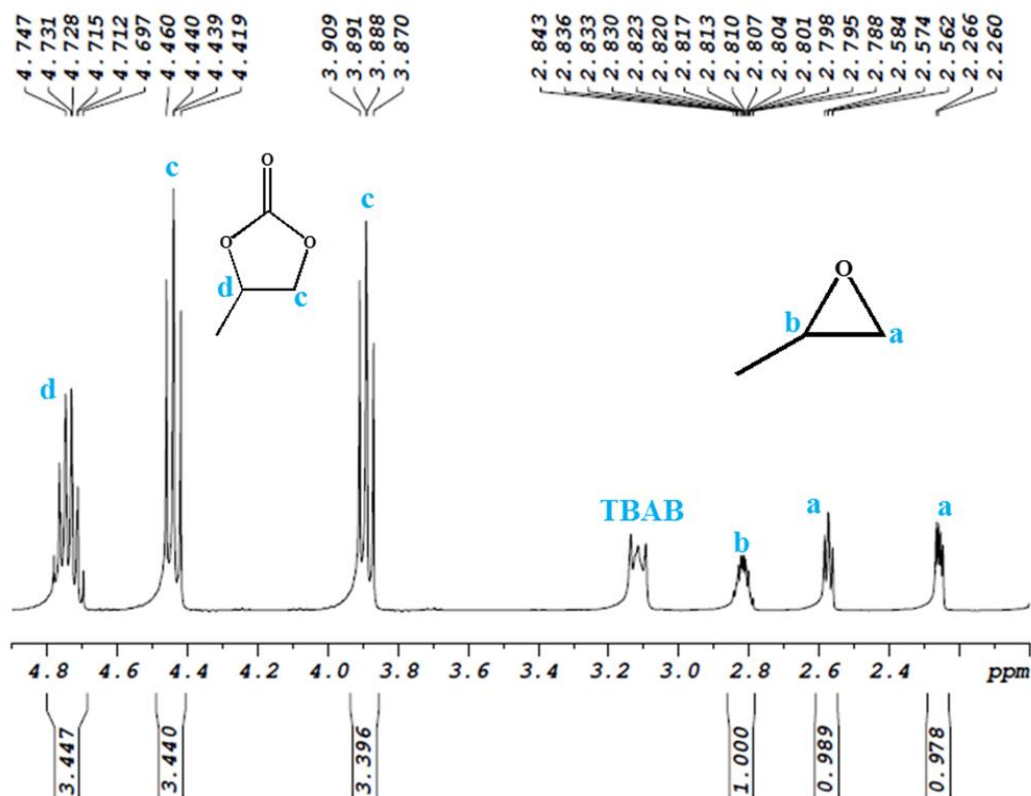


Fig. S20. ¹H-NMR spectra (in CDCl₃) of the reaction mixture using **CuBTC@AC-2** catalyst in the 2nd cycle of recyclability test.

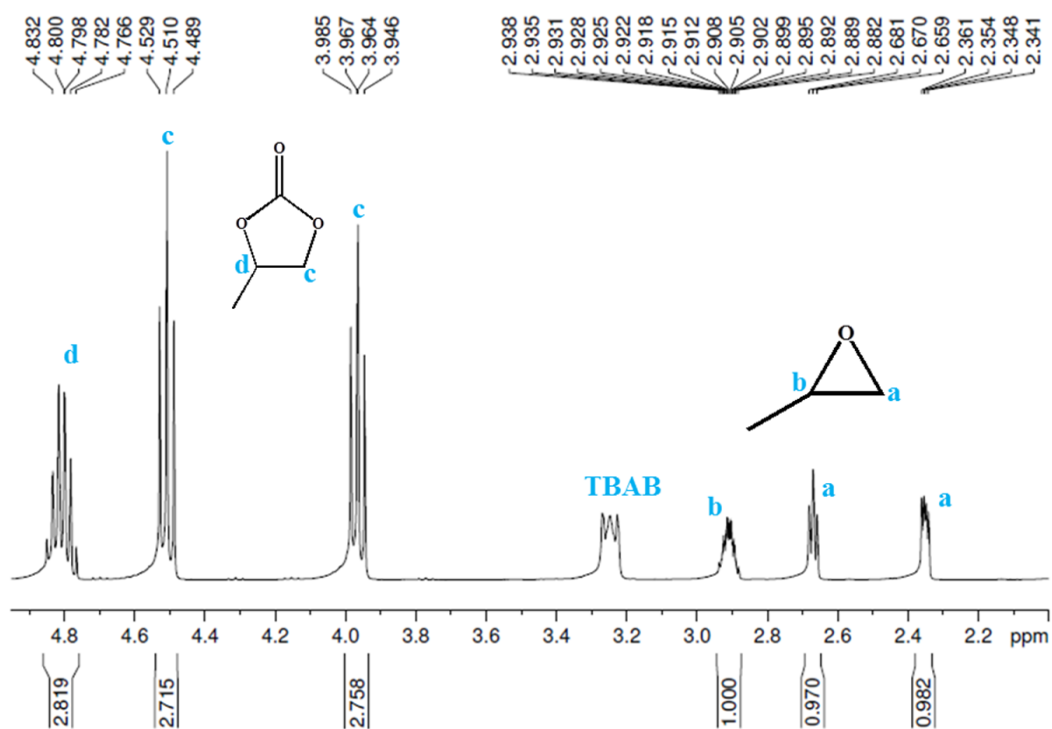


Fig. S21. $^1\text{H-NMR}$ spectra (in CDCl_3) of the reaction mixture using **CuBTC@AC-2** catalyst in the 3rd cycle of recyclability test.

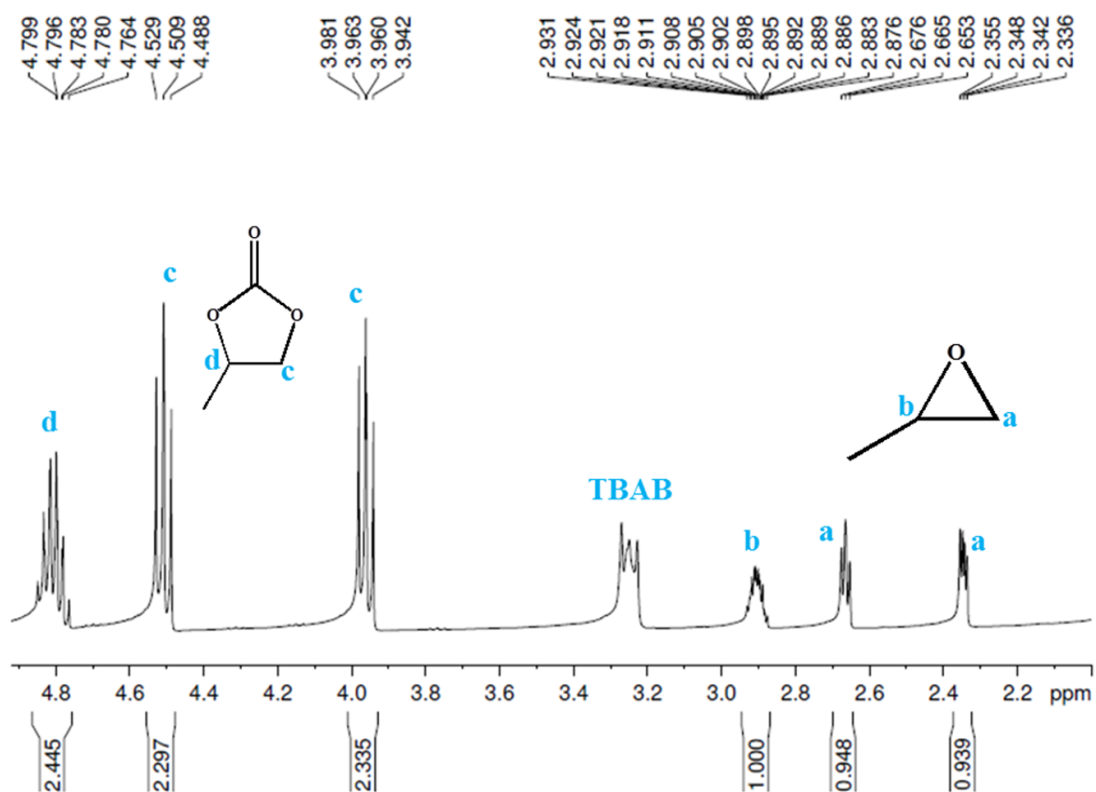


Fig. S22. $^1\text{H-NMR}$ spectra (in CDCl_3) of the reaction mixture using **CuBTC@AC-2** catalyst in the 4th cycle of recyclability test.

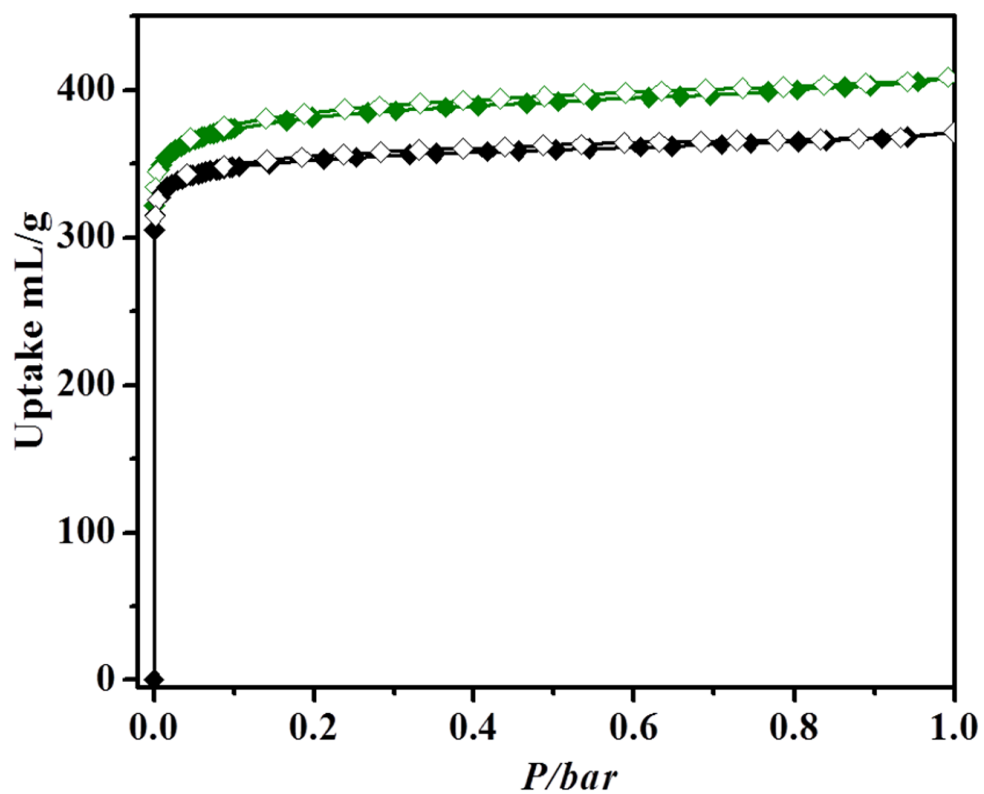


Fig. S23. N₂ adsorption isotherms at 77 K of activated pristine **CuBTC@AC-2** (green) and the sample recovered after 4th catalytic cycle (black). Open and closed symbol denotes adsorption and desorption respectively.